

Two-parameter Radial Equilibrium Models for Field-Reversed Configurations

H. J. Ma^{1,2,3}, H. S. Xie^{2,3*}, Y. K. Bai^{2,3}, S. K. Cheng^{2,3}, B. H. Deng^{2,3}, M. Tuszewski⁴, Y. Li^{2,3}, H. Y. Zhao^{2,3}, B. Chen^{2,3}, and J.Y. Liu^{1*}

¹ Key Laboratory of Materials Modification by Laser, Ion and Electron Beams (Ministry of Education), School of Physics, Dalian University of Technology, Dalian 116024, People's Republic of China

² Hebei Key Laboratory of Compact Fusion, Langfang 065001, People's Republic of China

³ ENN Science and Technology Development Co., Ltd., Langfang 065001, People's Republic of China

⁴ ENN Consultant, Riverside, CA 92506, USA

E-mail: *xiehuasheng@enn.cn, jyliu@dlut.edu.cn
13 October 2020

Abstract. A new equilibrium pressure profile extending the Rigid-Rotor (RR) model with a simple unified expression $P = P(\psi; \beta_s, \alpha, \sigma)$ for both inside and outside the separatrix is proposed, in which the radial normalized field-reversed configuration (FRC) equilibrium profiles for pressure, magnetic field, and current can be determined by only two dimensionless parameters $\beta_s \equiv P_s/2\mu_0 B_e^2$ and $\delta_s \equiv L_{ps}/R_s$, where P_s is the thermal pressure at the separatrix, B_e is the external magnetic field strength, L_{ps} is the pressure profile scale length at the separatrix, and R_s is the separatrix radius. This modified rigid rotor (MRR) model has sufficient flexibility to accommodate the narrow scrape of layer (SOL) width and hollow current density profiles, and can be used to fit experimental measurements satisfactorily. Detailed one-dimensional (1D) characteristics of the new MRR model are investigated analytically and numerically, and the results are also confirmed in two-dimensional (2D) numerical equilibrium solutions.

Submitted to: *Nucl. Fusion*

1 Introduction

Field-Reversed Configurations (FRC) are axisymmetric compact toroids with no or weak toroidal magnetic field ($B_\theta \approx 0$) [1–4]. Because of its simple configuration, intrinsically high β , existence of natural divertor structure, good stability, and also the attractive feature of without material objects linking the torus which allows the FRC to be translated along the cylindrical axis and to be compressed in separate vacuum chambers [3, 4], FRCs are often chosen as the advanced fuel fusion reactor design [5] or as the target plasma for magnetized target fusion (MTF) approach [3]. After formation, FRC plasmas are observed to be in stable equilibrium for many Alfvén transit times [6]. The detailed features of FRC equilibrium is of great significance to the research of instability, transport, and compression processes.

FRC is usually elongated cylindrical axisymmetric plasma, which can be well described in cylindrical coordinates with (r, θ, z) . It is generally accepted [1–4] that most FRC equilibria can be described by the Grad-Shafranov (G-S) equation. In cylindrical coordinates, with toroidal symmetry ($\partial/\partial\theta = 0$), the G-S equilibrium equation is:

$$\Delta^* \psi \equiv r \frac{\partial}{\partial r} \left(\frac{1}{r} \frac{\partial \psi}{\partial r} \right) + \frac{\partial^2 \psi}{\partial z^2} = -\mu_0 r^2 P'(\psi) \quad (1)$$

with

$$J_\theta = r P'(\psi) \quad (2)$$

$$B_z = \frac{1}{r} \frac{\partial \psi}{\partial r}; \quad B_r = -\frac{1}{r} \frac{\partial \psi}{\partial z} \quad (3)$$

where $B_\theta = 0$ is assumed, and $\psi = \Psi_p/2\pi = \int_0^r B_z r dr$ is the normalized radial magnetic flux, J_θ is the toroidal current density of plasma, P' is the derivative of pressure with respect to ψ and μ_0 is the vacuum permeability. Studies have shown that in present experiments kinetic effects of the equilibrium is small [7], and the FRC experimental study confirmed the applicability of the G-S equation [1, 8], at least for the inner region of FRCs.

As is shown above, the pressure profile determines the FRC's equilibrium. Various analytical pressure profile models, such as (extended) Hill's Vortex [9, 10], Rigid-Rotor (RR) [1, 11], extended Solov'ev [12], 2PE [13], and SYM [14] models, have been proposed for theoretical and experimental purposes. In numerical simulations, dozens of pressure expressions for the numerical solution of G-S equation have been proposed [3, 4,

15, 16]. Among these models, the RR model is the most widely adopted. However, it has the disadvantage of profile stiffness (i.e., when the parameter changes the shape of the profile remains essentially the same), which can lead to excess SOL thickness, and sometimes it is difficult to fit the experimental profile data with the RR model.

Recently, a 3PE model is proposed by Steinhauer [16], which is so far the most comprehensive $P(\psi)$ model for FRC equilibrium. However, the $P(\psi)$ form in the 3PE model is complicated and two piecewise expressions are used for the inner and outer regions, respectively, making it inconvenient to use. In this article, a two-parameter Modified RR model (MRR model) is proposed. It is constructed based on the RR model with a simple unified (instead of piecewise) expression $P = P(\psi; \beta_s, \alpha, \sigma)$, with the flexibility to allow for hollow or peaked current profiles, and flexible SOL width to match experimental measurements.

The outline of this paper is as follows. Section 2 introduces the formulation of the MRR model. The properties of the MRR model and the comparison of MRR with other models and experimental measurements are described in Section 3, where a new method for solving free parameters of the equilibrium model is also presented. FRC equilibrium in (β_s, δ_s) parameters space is explored in Section 4. 2D equilibrium based on the MRR model and solved using the GSEQ [17] code is presented in Section 5. Section 6 concludes with a summary and outlook to future work.

2 THE MRR EQUILIBRIUM MODEL

Although various models have been proposed to analyze the FRC experimental results, the RR model is the simplest one with clear physical meanings and is the most widely used [18, 19]. Therefore, the MRR pressure profile model $P = P(\psi)$ is based on the RR model, and is required to be as simple as possible, to have sufficient flexibility for fitting experimental data, and can be reduced to the RR model. In the following, the pressure profile in the RR model and the more recent 2PE and 3PE models are reviewed first, and then the pressure profile of the new MRR model is introduced.

The pressure expression of the RR model is

$$P = \frac{B_e^2}{2\mu_0} \cdot \text{sech}^2(K \cdot u) \quad (4)$$

where $u \equiv 2r^2/R_s^2 - 1$ is the familiar minor radius

variable, R_s is the separatrix radius, B_e is considered to be the vacuum magnetic field at the mid-plane, K is a free parameter. From Ref.[1], the following relation between radial flux ψ and r is obtained:

$$\cosh(K \cdot u) = \exp\left(\frac{4K}{B_e R_s^2} \psi\right) \cdot \cosh K, \quad (5)$$

From Eqs.(4) and (5), the pressure profile in the RR model can be written as a flux function as in Eq.(6), where $\beta \equiv P/(B_e^2/2\mu_0)$ is defined as the ratio between thermal pressure and magnetic pressure, and β_s is the separatrix value of β , with $\beta_s = \text{sech}^2(K)$ in the RR model[1].

As is well known that with a single parameter, the profiles in the RR model is quite stiff, and the current profile is always singly peaked from the geometry center to the boundary [Figs.1-2 and Ref.[16]]. The SOL width is also much larger than some experimental measurements [3]. Recently the more flexible 2PE and

3PE models are proposed. The normalized B_z inside of the separatrix of the 2PE[20] model is $b = b_s u e^{\sigma(u^2-1)}$ for $|u| \leq 1$. We define the direction so that $\psi < 0$ is inside of the separatrix (inner region), and $\psi > 0$ in the outer region (SOL), and $\psi = 0$ at the separatrix. The pressure profile $P(\psi)$ for the 2PE model is shown in Eq.(7). The $P(\psi)$ for a more complicated 2PE model[13] with $b = b_s u e^{\sigma(u^4-1)}$ for $|u| \leq 1$, is difficult to calculate analytically, thus not shown here. The pressure profile $P(\psi)$ of the 3PE[16] model inside the separatrix is given in Eq.(8). In Eqs.(7) and (8) b_s is the normalized magnetic field $b \equiv B(r)/B_e$ at the separatrix, σ and α are free parameters. In the 2PE and 3PE models [Eqs.(7) and (8)], the σ term can control the current density profile in polynomial form, such as the term $\left(\frac{8\psi\sigma}{B_e R_s^2 b_s} + 1\right)^2$ in 2PE model and the term $\frac{8\psi}{B_e R_s^2} \cdot \left(1 + \frac{1}{2} \frac{8\sigma}{B_e R_s^2} \psi\right)$ in 3PE model.

$$\text{RR:} \quad P(\psi) = \frac{B_e^2}{2\mu_0} \cdot \exp\left(-\frac{8K}{B_e R_s^2} \psi\right) \cdot \text{sech}^2(-K) = \frac{B_e^2}{2\mu_0} \cdot \beta_s \cdot \exp\left(-\frac{8K}{B_e R_s^2} \psi\right) \quad (6)$$

$$\text{2PE}(\psi \leq 0): \quad P(\psi) = \frac{B_e^2}{2\mu_0} \left\{ 1 - b_s^2 \left[\frac{1}{\sigma} \ln\left(\frac{8\psi\sigma}{B_e R_s^2 b_s} + 1\right) + 1 \right] \cdot \left(\frac{8\psi\sigma}{B_e R_s^2 b_s} + 1\right)^2 \right\}; \quad (7)$$

$$\text{3PE}(\psi \leq 0): \quad P(\psi) = \frac{B_e^2}{2\mu_0} \left\{ \beta_s - \frac{8\beta_s \alpha_1^2}{(7\alpha_1 - \sigma)} \left[\frac{8\psi}{B_e R_s^2} \left(1 + \frac{1}{2} \frac{8\sigma}{B_e R_s^2} \psi\right) + (\sigma + \alpha_1) \frac{1 - \exp\left(\frac{8\alpha_2}{B_e R_s^2} \psi\right)}{8\alpha_1^2} \right] \right\}; \quad (8)$$

$$\text{MRR:} \quad P(\psi) = \frac{B_e^2}{2\mu_0} \beta_s \cdot \exp\left[-\alpha \frac{\psi}{B_e R_s^2} - f_2(\psi)\right] \cdot f_1(\psi) + f_0(\psi); \quad (9)$$

$$\text{MRR-0:} \quad P(\psi) = \frac{B_e^2}{2\mu_0} \beta_s \cdot \exp\left(-\alpha \frac{\psi}{B_e R_s^2}\right) + f_0\left(\frac{\psi}{B_e R_s^2}; \sigma\right); \quad (10)$$

$$\text{MRR-1:} \quad P(\psi) = \frac{B_e^2}{2\mu_0} \beta_s \cdot \exp\left(-\alpha \frac{\psi}{B_e R_s^2}\right) \cdot \left[\sigma \left(\frac{\psi}{B_e R_s^2}\right)^q + 1\right]^n, \quad q = 1, n = 2 \text{ as default}; \quad (11)$$

$$\text{MRR-2:} \quad P(\psi) = \frac{B_e^2}{2\mu_0} \beta_s \cdot \exp\left[-\alpha \frac{\psi}{B_e R_s^2} - \sigma \left(\frac{\psi}{B_e R_s^2}\right)^n\right], \quad n = 2 \text{ as default}; \quad (12)$$

The 2PE and 3PE models are piecewise defined and complicated, difficult to use in practical applications. Therefore the RR model is modified to support adjustable current density profiles and SOL width. As shown in Eq.(9), new terms can be added to the RR model in three positions, denoted by f_0 , f_1 and f_2 respectively. Although the functions $f_i(\psi)$ with $i = 0, 1, 2$ can be arbitrary and coexist, we would consider the simplest case firstly, i.e., only one f_i exists and f_i is single parameter polynomial of ψ . Thus, a series of Modified RR (MRR) models are constructed in Eqs.(10)-(12). It will be shown later that these MRR models meet the requirements stated above. In these models, B_e and R_s are normalized scaling parameters and β_s , α and σ are parameters to control the radial FRC profile shapes. It should be noted that no strict relationship between α and β_s is assumed in the MRR model in contrast to the RR model. In order to distinguish different MRR

models, we identify them as MRR- i for different f_i with $i = 0, 1, 2$. The 3PE model can also be regarded as a special but complicated case of MRR-0 model. Physically, $P \rightarrow 0$ is required far off the separatrix ($\psi \rightarrow \infty$). However, it can be shown that $P(\psi \rightarrow \infty) \rightarrow \pm\infty$ in MRR-0 model, therefore another expression is needed in the open field line $\psi > 0$ region. This is also why the 3PE model requires separate expressions for the inner and outer regions. Hence in this work, only the MRR-1,2 models are studied in details. At the separatrix and geometry axis with $\psi = 0$, the pressure $P = \beta_s B_e^2/2\mu_0$. With $\sigma = 0$, $\alpha = 8K$ and $\beta_s = \text{sech}^2(K)$ in Eq.(11)-(12), the MRR model reduces to the RR model.

The current profile index (h), which describes the distribution property of current inside the separatrix of FRC equilibrium, is introduced in Ref.[21]:

$$h \equiv \frac{(j_{\theta}/r)_{O\text{-point}}}{\langle j_{\theta}/r \rangle} \quad (13)$$

where the averaging is calculated inside the separatrix in the mid-plane[13, 15]:

$$\langle j_\theta/r \rangle \equiv (1/\pi R_s^2) \int_0^{R_s} (j_\theta/r) 2\pi r dr. \quad (14)$$

The current density profile is “hollow” for $h < 1$, i.e. hollow at the magnetic axis, “flat” for $h = 1$, and “peaked” for $h > 1$. We will see in Figs.3- 6 that the current density profile of the MRR model can accommodate all three cases.

The following quantities would be useful in model applications:

$$\langle \beta \rangle = (1/\pi R_s^2) \int_0^{R_s} \beta 2\pi r dr, \quad (15)$$

$$I_{in} = \int_0^{R_s} j_\theta dr, \quad (16)$$

$$I_{total} = \int_0^\infty j_\theta dr, \quad (17)$$

$$c_i = I_{in}/I_{total}, \quad (18)$$

$$c_p = \frac{\int_0^{R_s} p r dr}{\int_0^\infty p r dr}, \quad (19)$$

which are the average β , line current density inside the separatrix, total current density, the fractional current inside the separatrix, and the fractional pressure integral inside the separatrix, which represent the fractional number of particles inside the separatrix assuming constant temperature, respectively. Using Eq.(16), the total current inside the separatrix under racetrack approximation can be calculated by multiplying the FRC length.

3 1D EQUILIBRIUM PROFILES OF THE MRR MODEL

The RR model has only one free parameter, as shown in Appendix A, where a more general relationship of $K = \log[\sqrt{\beta_s}/(\sqrt{1-\beta_s}+1)]$ is derived. For $\sigma = 0$, the MRR model is reduced to the RR model. Therefore, although it appears that the MRR model has three free parameters, it actually has only two. This is also true for the 3PE model. It is the constraint of the radial pressure balance that reduces one of the free parameter. In the following, a simple step-by-step method to solve the quasi-1D equilibrium is proposed in section 3.1. In section 3.2, the MRR model is applied to compare with experimental data. In section 3.3, general characteristics of 1D equilibrium profiles from the MRR model are presented.

3.1 A step-by-step method for quasi-1D equilibrium solution

Experimentally, R_s and B_e can be measured more easily than β_s and δ_s , where $\delta_s = L_{ps}/R_s$, with $L_{ps} = [P/(dP/dr)]_s$ being the pressure gradient-based SOL

width, and the subscript ‘s’ denotes the value in the mid-plane ($z = 0$) and at the separatrix ($r = R_s$). Therefore, β_s and δ_s are chosen to be the two free parameters in characterizing the 1D equilibrium.

The applicability of quasi-1D FRC equilibrium is discussed in Appendix B. In the quasi-1D equilibrium

$$P_m = P(\psi) + \frac{B_z^2}{2\mu_0} = \frac{B_e^2}{2\mu_0} \quad (20)$$

which yields $B_z = \pm\sqrt{2\mu_0[P_m - P(\psi)]}$. With $d\psi = rB_z dr$, and using B_z , we have

$$\begin{cases} -\frac{d\psi}{\sqrt{2\mu_0[P_m - P(\psi)]}} = r dr, r \leq R_0 \\ \frac{d\psi}{\sqrt{2\mu_0[P_m - P(\psi)]}} = r dr, r > R_0 \end{cases} \quad (21)$$

we thus can readily prove that $R_s = \sqrt{2}R_0$, with R_0 is the O-point radius. The pressure gradient scale length L_p is

$$L_p \equiv -\frac{P}{\frac{dP}{dr}} = -\frac{P(\psi)}{\frac{dP(\psi)}{d\psi} \cdot \frac{d\psi}{dr}}. \quad (22)$$

From Eq.(21), we obtain $d\psi/dr$ in the range of $r \leq R_0$

$$\frac{d\psi}{dr} = -r\sqrt{2\mu_0[P_m - P(\psi)]}. \quad (23)$$

At the O-point, the flux $\psi = \psi_m$ and pressure $P = P_m$, with ψ_m being the normalized trapped flux, therefore

$$P(\psi_m) = P_m. \quad (24)$$

The dimensionless forms are used for the radius $r/R_s \rightarrow r$, the pressure $P/P_m \rightarrow p$, SOL width $L_{ps}/R_s \rightarrow \delta_s$, the flux $\psi/(B_e R_s^2) \rightarrow \psi$ and the current density $J_\theta/J_m \rightarrow J_\theta$, with $J_m = B_e/(2\mu_0 R_s)$. Hereafter, unless otherwise stated, ψ means dimensionless flux, J_θ means dimensionless current density, r means dimensionless radius. Respectively the Eqs.(22), (24) and (21) are reduced to:

$$\delta_s = -\frac{p}{\frac{dp}{dr}} = -\frac{p(\psi)}{\frac{dp(\psi)}{d\psi} \cdot \frac{d\psi}{dr}} \quad (25)$$

$$p(\psi_m) - 1 = 0 \quad (26)$$

$$\int_0^{\psi_m} \frac{d\psi}{\sqrt{[1 - p(\psi_m)]}} + \frac{1}{4} = 0. \quad (27)$$

In terms of the normalized parameters defined above, Eq.(25) can be written in different forms for each model described by Eqs.(6)-(12):

$$\text{RR:} \quad 8\delta_s \log\left(\frac{\sqrt{1-\beta_s}+1}{\sqrt{\beta_s}}\right) \sqrt{1-\beta_s} - 1 = 0 \quad (28)$$

$$\text{MRR-1:} \quad \begin{cases} \delta_s(\alpha - n\sigma)\sqrt{1-\beta_s} - 1 = 0; & q = 1 \\ \delta_s\alpha\sqrt{1-\beta_s} - 1 = 0; & q \neq 1 \end{cases} \quad (29)$$

$$\text{MRR-2:} \quad \delta_s\alpha\sqrt{1-\beta_s} - 1 = 0 \quad (30)$$

$$\text{2PE:} \quad 8\delta_s(1-\beta_s)(1+2\sigma) - \beta_s = 0 \quad (31)$$

$$\text{3PE:} \quad \delta_s 16\alpha(3\alpha - \sigma)\sqrt{1-\beta_s} + (7\alpha - \sigma) = 0 \quad (32)$$

The following steps are used to solve the constraint equations: First, the α parameter is solved from Eqs.(28)-(32) from specified δ_s and β_s ; second, the intermediate variable of trapped flux ψ_m is solved from Eq.(26); third, Eq.(27) is solved as $F(\sigma) = 0$ to obtain σ ; and finally all the other parameters are obtained and $P(\psi)$ is determined. Subsequently the FRC profiles such as $p(r)$, $B_z(r)$, $\psi(r)$ and $j_\theta(r)$ are determined.

3.2 Model comparison by fitting to the experimental data

From the above discussions, it is shown that equilibrium profiles can be determined by a set of parameters (β_s, δ_s). To compare different models, they are used to fit the experimental data from FRC experiments of NUCTE-III[22, 23] and FRX-C[24].

The normalized pressure profile in NUCTE-III device is represented by the measured normalized bremsstrahlung intensity profile as shown in Fig.1a by the crosses. Bremsstrahlung radiation intensity is proportional to the square of density, and is a complicated function of T_e . In FRC plasmas, T_e profile is quite flat within the separatrix[3, 25]. Therefore, the normalized bremsstrahlung intensity profile can be considered to be proportional to the square of the pressure. In Fig.1a, quasi-1D equilibrium pressure squared from each model that best fit the experimental data are plotted. It is shown that the RR model cannot fit the experimental data with broad peak. This shows the disadvantage of profile stiffness of the RR model. It is also shown that within $r < 0.5$, the curve fit of the 2PE model deviates from the data more than the MRR models and the 3PE model. The difference between the MRR models and the 3PE model is small. However, the MRR models have unified expression for both inside and outside the separatrix and are more convenient for applications. It should be noted that the 2PE, 3PE and s-f profile are given by segmented expressions presented in Refs.[16, 20, 23]. The s-f profile is just proposed to fit the the experimental measurement in Ref.[23], meanwhile, the profile is a segmented expressions of r , which is not applicable to the G-S equation, so we will not study it further in the following. Fig.1b compares the current density profiles of difference models. The RR model shows a single peak, which is inconsistent with the broad experimental pressure profile shown in Fig.1a. The MRR models and the 3PE model yield similar hollow current profiles, while the 2PE model yields a much sharper current density peak near the separatrix. In equilibrium the pressure gradient is maintained by the $J \times B$ force. The broad pressure profile indicates the existence of a gradient minimum and is consistent with the hollow current density profiles from the MRR and 3PE models.

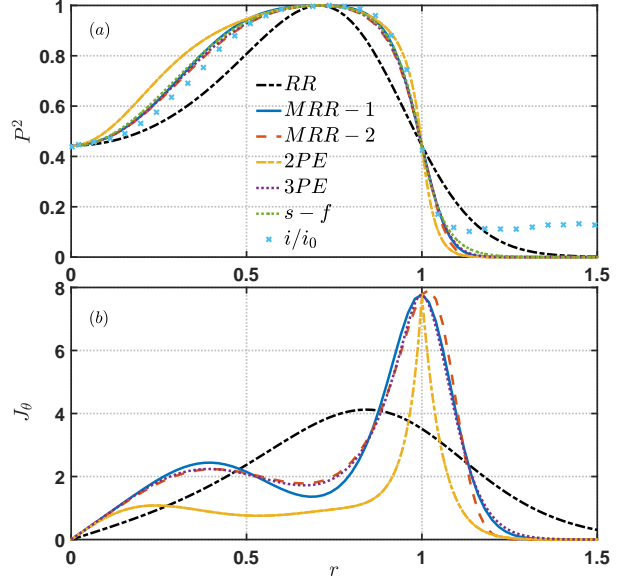


Figure 1. The radial profiles of the RR, MRR-1,2, 2PE, 3PE and s-f models for NUCTE-III experimental parameters ($\beta_s = 0.6655, \delta_s = 0.148$). (a) is the radial profile of bremsstrahlung intensity $i(r)/i_0$ from NUCTE-III[23] and the squares of pressures P^2/P_m^2 of models, (b) is the toroidal current density. $K = 0.66$ and $R_s = 5.61\text{cm}$ is set.

The normalized experimental density profile of the FRX-C device from Ref.[24] is reproduced in Fig.2a, represented by the crosses. Assuming uniform electron temperature profile inside the separatrix, the shape of the pressure profile is close to the density profile. Therefore, the pressure profile of each model can be used to fit the measured density profile as shown in Fig.2a. It is shown that the MRR and 3PE models fit the experimental data well inside the separatrix while the fit of the 2PE and RR models are not satisfactory. The current density profiles of difference models is also presented in Fig.2b. Like Fig.1b, the RR model shows a single peak, and the 2PE model shows a great difference with the MRR and 3PE models, which displays the consistent results with Fig.2a.

The MRR-1,2 and 3PE models also agree with each other well outside the separatrix, but are obviously different from the experimental density profile. One possible reason is that the temperature profile is not constant but decreasing rapidly outside the separatrix[25], which causes the pressure profile to drop faster than the density profile. We have also checked with other experimental results, for examples the density profiles from Refs.[8, 26], and similar conclusions can be obtained. More restricted comparison between measured FRC profiles and the models should be done when more experimental data become available.

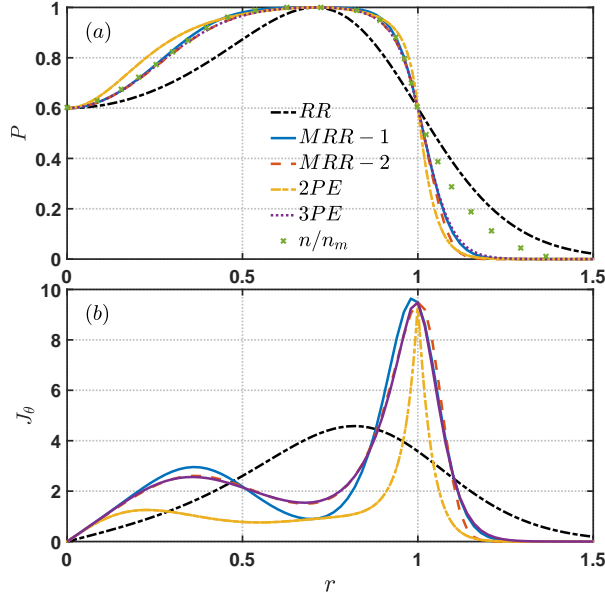


Figure 2. The radial profiles of the RR, MRR-1,2, 2PE and 3PE models for FRX-C experimental parameters ($\beta_s = 0.60, \delta_s = 0.10$). (a) is pressure profile from FRX-C experiment[24] with the constant temperature and the matched pressure profile of models. (b) is the toroidal current density.

3.3 1D characteristics of MRR models

From Figs.1 and 2, it is found that the 3PE model is very close to MRR-2 model in the inner region and close to MRR-1 model at the outer region. So, the 3PE model is between MRR-1 and MRR-2 models. Thus in this subsection, only the properties of MRR-1 and MRR-2 models are studied in details.

Fig.3 shows the evolution of the radial profiles with the change of δ_s of MRR-1 model when β_s is kept constant. As shown in Fig.3a, with the decreases of δ_s , the pressure profile become sharper in the outer region and flatter in the inner region of the FRC. The current density profile gradually changes from peak to hollow as shown in Fig.3b. The changes in magnetic flux ψ and magnetic field B_z are shown in Fig.3c and 3d respectively. These results show that when the current profile peaks sharply at the separatrix, the pressure gradient is sharp there, while the pressure peak is broad inside the separatrix, corresponding to the hollow current profile inside, which can be understood via the relation $J_\theta = rP'(\psi)$. Similar results are obtained from the MRR-2 model with the variation of δ_s as shown in Fig.4.

Fig.5 shows the evolution of the radial profiles with β_s of MRR-1 model for constant δ_s . As shown in Fig.5a, with the decreases of β_s , the pressure profile becomes flatter in the outer region and sharper in the inner region of the FRC. The current density profile gradually changes from hollow to peak is shown in Fig.5b. The

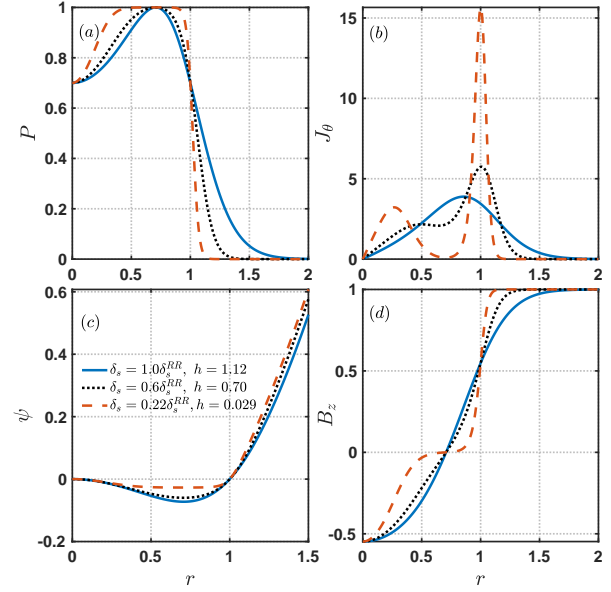


Figure 3. The radial profiles of MRR-1 model using $n = 2, q = 1$ with ($\beta_s = 0.7, \delta_s^{RR} = 0.37$). (a) is the pressure P , (b) is the current density J_θ , (c) is the magnetic flux ψ and (d) is the magnetic field B_z . δ_s^{RR} is the RR model's δ_s , h is the definition of Eq.10.

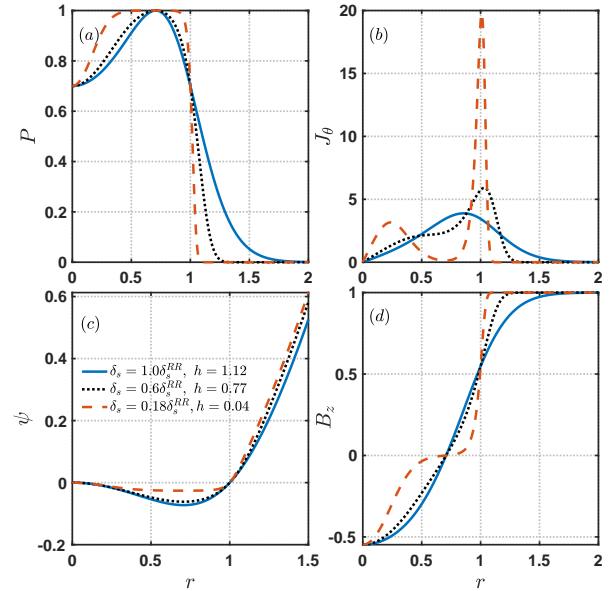


Figure 4. The radial profiles of MRR-2 model using $n = 2$ with ($\beta_s = 0.7, \delta_s^{RR} = 0.37$). (a) is the pressure P , (b) is the current density J_θ , (c) is the magnetic flux ψ , and (d) is the magnetic field B_z . δ_s^{RR} is the RR model's δ_s , h is the definition of Eq.10.

changes in magnetic flux ψ and the magnetic field B_z are also presented in Fig.5c and 5d respectively. Similar results are obtained from the MRR-2 model with the variation of β_s as shown in Fig.6.

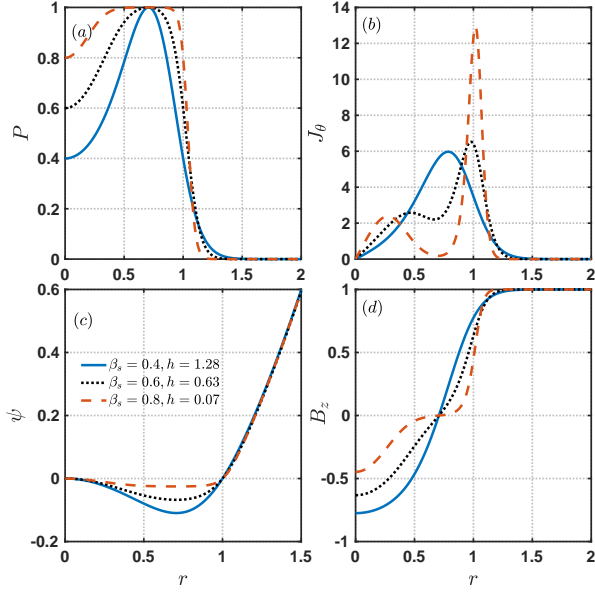


Figure 5. The radial profiles of MRR-1 model using $n = 2, q = 1$ with $\delta = 0.148$. (a) is the pressure P , (b) is the current density J_θ , (c) is the magnetic flux ψ and (d) is the magnetic field B_z .

We also observed in Figs.3- 6 that the differences between the radial profiles of MRR-1 and MRR-2 are very small for a wide range of β_s and δ_s . Thus again, the MRR models are robust. This implies that, instead of the form of $P(\psi)$, the parameters (β_s, δ_s) is much important to determine the FRC radial profiles, which is the most interesting finding in this work. Hence, we think the two parameters (β_s, δ_s) can describe FRC radial equilibrium completely to a very high accuracy. That is, after two values (β_s, δ_s) is given, a FRC equilibrium with profiles $\psi(r)$, $p(r)$, $J_\theta(r)$ and $B_z(r)$ is uniquely determined! This feature would simplify the FRC equilibrium reconstruction or fitting a lot.

4 FRC EQUILIBRIUM IN (β_s, δ_s) PARAMETERS SPACE

It is shown in Section 3 that a set of parameters (β_s, δ_s) can represent FRC radial equilibrium uniquely for models with less than three free parameters, it would be useful to calculate other model parameters in the (β_s, δ_s) parameters space. It is limited to the MRR-1 model in this section. These results can be used for future theoretical or experimental studies directly. Fig.7 shows the contour of quantities in the (β_s, δ_s) space using the MRR-1 model. The upper limit in the (β_s, δ_s) space is the RR model and the lower

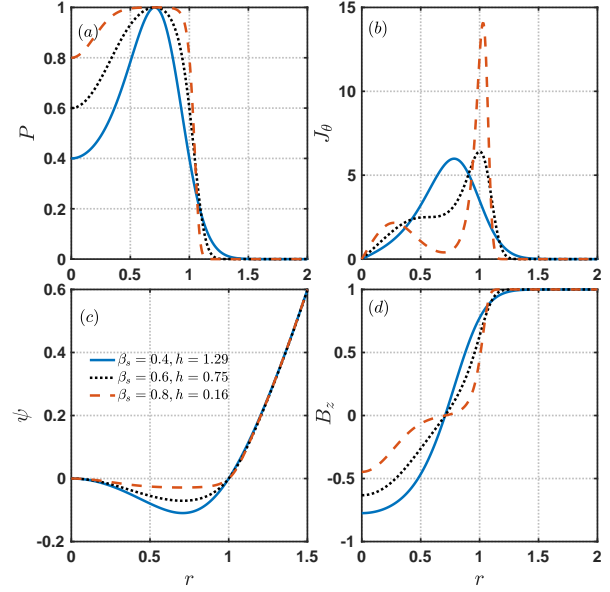


Figure 6. The radial profiles of MRR-2 model using $n = 2$ with $\delta = 0.148$. (a) is the pressure P , (b) is the current density J_θ , (c) is the magnetic flux ψ and (d) is the magnetic field B_z .

line corresponds to $h = 0$, h is defined in Eq.13. In FRC experiments, real-time rapid reconstruction of equilibrium is desired, after the values of (β_s, δ_s) is given in the experiment, the equilibrium quantities including the trapped flux (ψ_{min}), the current profile index (h), the average β ($\langle\beta\rangle$) can be estimated quickly using Figs.7a, 7d, and 7e respectively, the current of plasma inside the separatrix, the ratio of current and the number of particles inside the separatrix are also given in Figs.7f, 7g and 7h. Meanwhile, Figs.7b and 7c can provide a set of initial free parameters (α, σ) for accurate FRC equilibrium reconstruction.

5 MRR MODEL APPLIED TO 2D EQUILIBRIUM STUDIES

The GSEQ (General Solver for EQUilibrium) code is developed by the ENN theory and simulation group to study 2D FRC equilibrium properties by solving the G-S equation[17] under fixed or free boundary conditions. Conducting cylindrical fixed boundary is used as upper wall conditions in the current version. The detailed description of the code and more 2D studies of the MRR-1,2 model will be presented in future publications. Here 2D FRC equilibrium with the MRR-1 model is solved by the GSEQ code and compared with the quasi-1D result in Fig.8. The MRR-1 model parameters chosen are $q = 1, n = 2$. The NUCTE-III device geometric parameters are used. It should be noted that the 2D result of MRR-1 is obtained using the same free parameters as in the 1D model with only the iteration of ψ . From Fig.8b-

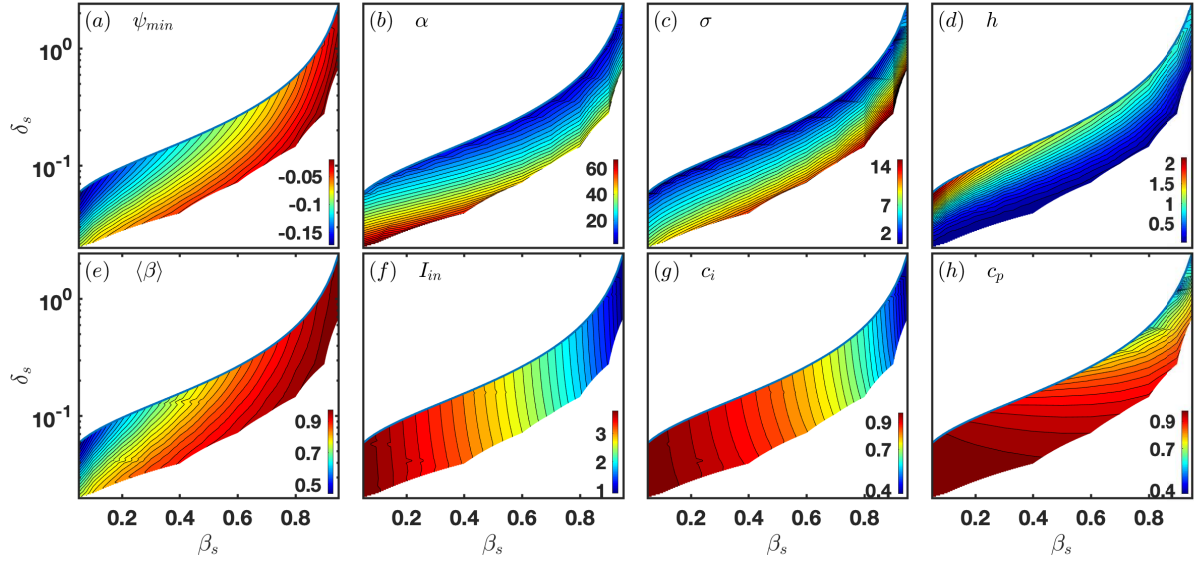


Figure 7. The contour of other quantities in (β_s, δ_s) space are shown. Trapped flux ψ_{min} is (a), the parameters α is (b), the parameters σ is (c), the current profile index h is (d), the average β $\langle\beta\rangle$ is (e), the line current density inside the separatrix with Eq.16 is (f), the ratio of current inside the separatrix with Eq.18 is (g) and the ratio of pressure inside the separatrix with Eq.19 is (h).

d, it is seen that the 1D and 2D results of the MRR-1 model agree with each other well. Similar comparison shows that the 1D and 2D results of the MRR-2 model also agrees well. This means that the MRR-1,2 model is suitable for 2D FRC equilibrium reconstruction and the quasi-1D equilibrium holds well in the mid-plane.

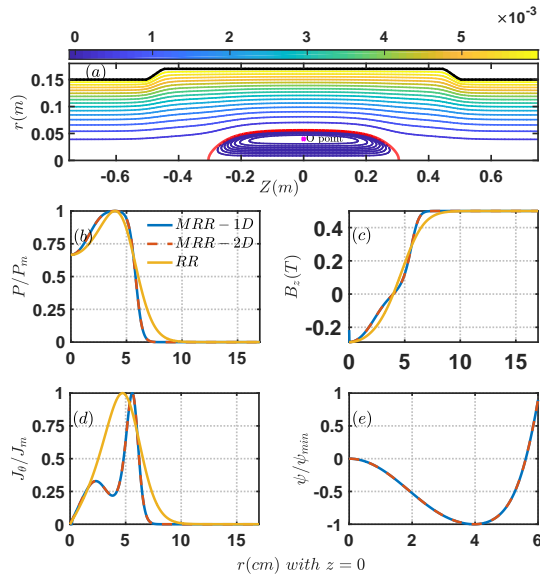


Figure 8. The 2D contour of ψ for NUCTE-III device and the comparison of the 1D and 2D radial profiles of MRR-1 model. (a) is the 2D contour of ψ , (b) is the radial pressure P/P_m , and (c) is the B_z profile, (d) is current density J_θ/J_m profile at the mid-plane and (e) is ψ .

6 SUMMARY AND CONCLUSION

A modified rigid rotor FRC equilibrium pressure profile model $P(\psi; \beta_s, \alpha, \sigma)$ with unified simple expression for both inside and outside the separatrix is developed. With two free parameters, which can be conveniently chosen to be the normalized SOL width and the separatrix β value, this model eased the difficulty of profile stiffness of the RR model. The MRR model is easy to solve with a simple step-by-step method, and is used to study the 1D and 2D FRC equilibrium properties. This model shows its advantages in fitting the experimental profiles with broad pressure peak and sharp gradient near the separatrix. In the future, FRC equilibrium fitting (FRC-EFIT) code can be developed based on the MRR model. Also, a more accurate study of some analytical approximated axial pressure equilibrium relations such as the Barnes average β relation[27] and the trapped flux relation[3] will be a future topic.

Acknowledgments

This work is supported by the China central government guides the development of local science and technology funding No.206Z4501G and the compact fusion project of the ENN group.

Appendix A THE RR MODEL HAS ONLY ONE FREE PARAMETER

The normalized pressure as a flux function ψ in RR model is[1]:

$$p(\psi) = \beta_s \cdot \exp(-K\psi); \quad \beta_s = \text{sech}^2(K) \quad (\text{A.1})$$

where the pressure is normalized by the external magnetic pressure $B_e^2/2\mu_0$, the flux is normalized by $B_e R_s^2$. We show in the following that the relationship between β_s and K is a consequence of radial pressure balance, and therefore, the RR model has only one free parameter.

Consider a more general normalized expression:

$$p(\psi) = \beta_s \exp(-b\psi) \quad (\text{A.2})$$

with two free parameters β_s and b .

Eq.(A.3) is obtained from radial pressure balance[1]:

$$\frac{d\psi}{-\sqrt{1-\beta_s \exp(-b\psi)}} = \frac{r^2}{2}, \quad 0 \leq r \leq R_0 \quad (\text{A.3})$$

Integrate Eq.(A.3), with the integration formula:

$$\int \frac{1}{\sqrt{1-me^{-nx}}} dx = \frac{2 \log \left[\sqrt{e^{nx} - m} + e^{\frac{nx}{2}} \right]}{n} \quad (\text{A.4})$$

it can be obtained

$$\begin{aligned} & \sqrt{e^{b\psi} - \beta_s} + \exp\left(\frac{b\psi}{2}\right) \\ &= \exp\left[-\frac{r^2}{4}b + \log[\sqrt{1-\beta_s} + 1]\right] \end{aligned} \quad (\text{A.5})$$

Setting $y \equiv \exp(b\psi/2)$ and

$$c \equiv \exp\left[-\frac{r^2}{4}b + \log[\sqrt{1-\beta_s} + 1]\right] \quad (\text{A.6})$$

the Eq.(A.5) is simplified to

$$\sqrt{y^2 - \beta_s} = c - y. \quad (\text{A.7})$$

Solving Eq.(A.7) to obtain $y = (c^2 + \beta_s)/2c$, thus

$$\psi = \frac{2}{b} \log \left\{ \frac{c^2 + \beta_s}{2c} \right\}. \quad (\text{A.8})$$

At the O point with $r_0 = 1/\sqrt{2}$, $P(\psi) = 1$, then

$$\left\{ \frac{c^2 + \beta_s}{2c} \right\}^{-2} = \frac{1}{\beta_s}. \quad (\text{A.9})$$

So $c^2 = \beta_s$, which is

$$\left[\sqrt{1-\beta_s} + 1 \right]^2 \exp\left[-\frac{r^2}{2}b\right] = \beta_s. \quad (\text{A.10})$$

Then, we obtain

$$b = -\frac{2}{r_0^2} \log \left(\frac{\beta_s}{[\sqrt{1-\beta_s} + 1]^2} \right). \quad (\text{A.11})$$

Define $d \equiv c/\sqrt{\beta_s}$, Eq.(A.2) can be written as

$$\begin{aligned} P(r) &= \beta_s \exp\left(-2 \log \left\{ \frac{c^2 + \beta_s}{2c} \right\}\right) = \left\{ \frac{2}{d + d^{-1}} \right\}^2 \\ &= \text{sech}^2 \left[\log \left(\frac{\sqrt{\beta_s}}{[\sqrt{1-\beta_s} + 1]} \right) (2r^2 - 1) \right] \end{aligned} \quad (\text{A.12})$$

with

$$d = \exp \left[\log \left(\frac{\sqrt{\beta_s}}{[\sqrt{1-\beta_s} + 1]} \right) (2r^2 - 1) \right] \quad (\text{A.13})$$

From Eq.(A.12), we conclude that the general pressure expression $p = \beta_s \exp(-b\psi)$ has only one free parameter and is actually identical to the RR model.

Appendix B THE ACCURACY OF QUASI-1D EQUILIBRIUM

FRC is elongated along the cylindrical axis, and often considered as in 1D equilibrium when the curvature force at the mid-plane is neglected, leading to the following "pressure balance" equation:

$$P + \frac{B_z^2}{2\mu_0} = \frac{B_e^2}{2\mu_0} \quad (\text{B.1})$$

It is interesting to check the accuracy of the quasi-1D equilibrium. The force balance equation without approximation is:

$$\mathbf{J} \times \mathbf{B} = \nabla P, \quad (\text{B.2})$$

In cylindrical coordinates (r, θ, z) , it can be written as:

$$J_\theta B_z - J_z B_\theta = \frac{\partial P}{\partial r}. \quad (\text{B.3})$$

For ideal FRC with $B_\theta = 0$, using Ampere's law, $\mu_0 \mathbf{J} = \nabla \times \mathbf{B}$, Eq.(B.3) is integrated to yield:

$$P + \frac{B_z^2}{2\mu_0} = \frac{B_e^2}{2\mu_0} + \int \frac{B_z}{\mu_0} \left(\frac{\partial B_r}{\partial z} \right) dr \quad (\text{B.4})$$

where B_e is the external magnetic field, and the last term representing the curvature effect is neglected in the quasi-1D equilibrium. The significance of this term is estimated below. Define:

$$\delta \equiv \frac{\int \frac{B_z}{\mu_0} \left(\frac{\partial B_r}{\partial z} \right) dr}{\frac{B_e^2}{2\mu_0}} = \frac{2}{B_e^2} \int B_z \left(\frac{\partial B_r}{\partial z} \right) dr. \quad (\text{B.5})$$

In experiments the FRC separatrix is elliptical in shape. To estimate the value range of δ , Hill's vortex model with elliptical separatrix is used, where the flux contour is

$$\psi = \frac{B_0}{2} r^2 \left(1 - \frac{r^2}{a^2} - \frac{z^2}{b^2} \right) \quad (\text{B.6})$$

where $B_0 = B_e \sqrt{1-\beta_s}$ is the magnetic field at the separatrix. in the mid-plane,

$$\delta = \frac{B_0^2}{B_e^2 b^2} r^2 \left(1 - \frac{r^2}{a^2} \right). \quad (\text{B.7})$$

The maximum value of δ can be expressed in term of FRC elongation $E = b/a$:

$$\delta < \delta_c = \frac{1 - \beta_s}{4E^2} \quad (\text{B.8})$$

In current FRC experiments, typical E value range is 3 – 10. From Eq.(B.8), when $E > 2$, $\delta < 1/16$, which means that the magnetic field curvature has little effect on the radial balance and quasi-1D equilibrium is a good approximation for FRC plasmas. Fig.B1 plotted more detailed estimation of δ for typical FRC β_s and elongation parameters, and in most cases $\delta_c < 1\%$.

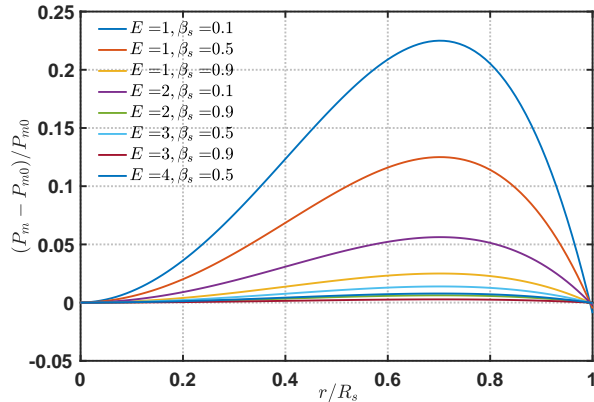


Figure B1. The effect of FRC elongation with Hill's model, which represents the accuracy of quasi-1D equilibrium.

References

[1] W. Armstrong, R. Linford, J. Lipson, D. Platts, and E. Sherwood, *The Physics of Fluids* **24**, 2068 (1981).
 [2] J. Finn and R. Sudan, *Nuclear Fusion* **22**, 1443 (1982).
 [3] Tuszewski and M., *Nuclear Fusion* **28**, 2033 (1988).
 [4] L. C. Steinhauer, *Physics of Plasmas* **18**, 070501 (2011).
 [5] M. W. Binderbauer, H. Y. Guo, M. Tuszewski, S. Putvinski, L. Sevier, and E. Al, *Physical Review Letters* **105**, 045003 (2010).
 [6] R. Spencer and M. Tuszewski, *The Physics of fluids* **28**, 1810 (1985).
 [7] R. Webster, J. Schwarzmeier, H. Lewis, C. Choi, and W. Terry, *Physics of Fluids B: Plasma Physics* **3**, 1026 (1991).

[8] S. Okada, Y. Kiso, S. Goto, and T. Ishimura, *Journal of applied physics* **65**, 4625 (1989).
 [9] R. L. Spencer and D. W. Hewett, *The Physics of Fluids* **25**, 1365 (1982).
 [10] L. C. Steinhauer, *Physics of Fluids B: Plasma Physics* **2**, 3081 (1990).
 [11] R. Morse and J. Freidberg, *The Physics of Fluids* **13**, 531 (1970).
 [12] A. J. Cerfon and J. P. Freidberg, *Physics of Plasmas* **17**, 032502 (2010).
 [13] L. C. Steinhauer and T. Intrator, *Physics of Plasmas* **16**, 072501 (2009).
 [14] K. Lee, *Nuclear Fusion* **60**, 046010 (2020).
 [15] R. Kanno, A. Ishida, and L. C. Steinhauer, *Journal of the Physical Society of Japan* **64**, 463 (1995).
 [16] L. Steinhauer, *Physics of Plasmas* **21**, 082516 (2014).
 [17] H. Xie, *MHD Equilibrium Solver GSEQ*, Tech. Rep. (ENN (China), 2019).
 [18] B. Deng, J. Douglass, T. Roche, E. Belova, M. Beall, M. Binderbauer, R. Clary, S. Dettrick, H. Gota, E. Granstedt, et al., *Nuclear Fusion* **58**, 126026 (2018).
 [19] F. Conti, F. Wessel, M. Binderbauer, N. Bolte, F. Giammanco, M. Morehouse, A. Qerushi, H. Rahman, T. Roche, and M. Slepchenkov, *Physics of Plasmas* **21**, 022511 (2014).
 [20] L. Steinhauer, *Physics of Plasmas* **15**, 012505 (2008).
 [21] L. C. Steinhauer and A. Ishida, *Physics of Fluids B: Plasma Physics* **4**, 645 (1992).
 [22] Y. Ohkuma, M. Urano, M. Nakamura, Y. Narushima, T. Takahashi, and Y. Nogi, *Nuclear fusion* **38**, 1501 (1998).
 [23] T. Ikeyama, M. Hiroi, Y. Nogi, and Y. Ohkuma, *Physics of Plasmas* **16**, 042512 (2009).
 [24] M. Tuszewski, *Plasma physics and controlled fusion* **26**, 991 (1984).
 [25] B. Deng, J. Kinley, and J. Schroeder, *Review of Scientific Instruments* **83**, 10E339 (2012).
 [26] K. Suzuki and S. Hamada, *Journal of the Physical Society of Japan* **55**, 3705 (1986).
 [27] D. Barnes, C. Seyler, and D. Anderson, *Compact torus theory: MHD equilibrium and stability*, Tech. Rep. (Los Alamos Scientific Lab., NM (USA), 1979).